POLITECNICO DI TORINO
Repository ISTITUZIONALE

Application of digital image correlation in operational modal analysis of rotating structures

Original
Application of digital image correlation in operational modal analysis of rotating structures / Occhipinti, S., Mastrodicasa, D., Manzato, S., Di Lorenzo, E.. - ELETTRONICO. - (2024), pp. 2544-2555. (ISMA 2024 International Conference on Noise and Vibration Engineering Leuven (BEL) 9-11 September 2024).

Availability:
This version is available at: 11583/2996376 since: 2025-01-08T12:56:21Z

Publisher:
KU Leuven - Department of Mechanical Engineering

Published
DOI:

Terms of use:

This article is made available under terms and conditions as specified in the corresponding bibliographic description in the repository

Publisher copyright

(Article begins on next page)

14 November 2026

Local digital image correlation algorithms: spatial domain versus frequency domain approach

P. Neri [1], A. Paoli [1], S. Occhipinti [2], C.M. Firrone [2], D. Botto [2]
[1] Unviersity of Pisa, Department of Mechanical Engineering,
Largo L. Lazzarino 1, 56123, Pisa, Italy
e-mail: **paolo.neri@unipi.it**

[2] Politecnico di Torino, Department of Mechanical and Aerospace Engineering
Corso Duca degli Abruzzi, 24, 10129 Turin, Italy

Abstract
Digital image correlation (DIC) is widespread in many research fields to achieve full-field displacement measurements. The main idea behind the DIC method is the computation of the correlation factor between image subsets before and after deformation to assess the rough displacement. The correlation map, which is computed at the pixel level, is then refined to subpixel accuracy through interpolation methods or non-linear optimization. The aim of this research is to develop two digital image correlation algorithms for vibration measurements. The first will be based on the conventional approach, which computes the correlation factor in the spatial domain by convoluting the pixel-wise grey levels to obtain the correlation map. The second will be based on the computation of the correlation factor in the "frequency" domain. The algorithms will be evaluated in terms of performance when applied to the same image set, by comparing the computational time, and the sensitivity to small amplitude values, which are typical of vibrations.

1 Introduction

Digital Image Correlation (DIC) is an optical technique widely adopted in experimental mechanics to compute full-field data of a specimen's surface from a series of captured images. This method involves monitoring the movement of features generated by a grayscale speckle pattern applied to the specimen's surface, which undergoes varying loading conditions [1]. The subsequent image-processing stage exploits correlation-based algorithms to match corresponding subsets within a sequence of digital images, allowing the computation of full-field displacement and strain maps over time. When stereo-vision setups are used, the matching of subsets in image pairs enables the reconstruction of three-dimensional geometries (3D-DIC) [2]. The core principle of the DIC method relies on determining the correlation factor between image subsets of the target surface undergoing motion or deformation. The correlation map is used to estimate the approximate displacement of the image features. This is done initially at the pixel level and then at the sub-pixel level using interpolation techniques or non-linear optimization methods. Typically, algorithms based on iterative cross-correlation in the spatial domain (e.g., nonlinear Newton–Raphson method for least squares regression) are used. Scientific literature has also focused on refining the correlation criteria (e.g., the sum of squared difference (SSD), the zero-mean normalized sum of squared difference (ZNSSD)) [3], the grey-level interpolation function and the shape functions used to approximate the local deformation of the deformed subsets [2]. An alternative approach to detect displacements between speckle patterns is to operate in the frequency (spatial-frequency) domain [4, 5]. The Fourier transform can be used to convert the image's grayscale distribution function, which describes the intensity values of each pixel, into a frequency distribution. In the frequency domain search method, the frequency components of an image serve as metrics indicating the magnitude of variations in grayscale values within the image. According to the Fourier transforms theory (convolution theorem), the cross-correlation operation in the spatial domain is equivalent

to a simple product in the frequency domain [5]. Shifting the analysis from the spatial to the frequency domain then allows avoiding the pixel-by-pixel matching process, which is slow, introducing a simple product operation, which is faster. However, the spatial-frequency approach is not free from drawbacks. First, decorrelation may occur for relatively large displacements since the same area is processed at two different times (before and after loading) and thus the considered templates do not perfectly identify the same area of the sample. Second, the Nyquist criterion dictates the maximum detectable displacement, which is limited to half the size of the subset to avoid aliasing phenomena. Finally, frequency domain methods can be more sensitive to noise, especially high-frequency noise, which can interfere with the correlation process thus reducing accuracy [6]. Scientific literature that compares different DIC methods in spatial and frequency domains is quite limited. In [6], such a comparison is carried out, but it is focused on geoscience applications. In [7], the analysis of speckle patterns in both domains is used to characterize polyethylene films undergoing tensile deformation.
In the present work, a comparison of DIC algorithms operating in spatial and frequency domains is presented, in terms of computational costs and sensitivity to small amplitude displacements. Synthetic and experimental datasets have been used. In particular, experimental data have been acquired from a target surface undergoing high-frequency vibration. High-frequency responses of mechanical components are usually characterized by complex shapes and small displacements, which can fall in the range of 0.01 pxl. For this reason, it is essential to achieve high sensitivity, especially in the presence of image noise, to obtain precise analyses and reliable results. Finally, a hybrid approach is proposed by combining algorithms working in both domains on the basis of the measured displacement value, to push on computational time and or sensitivity.

2 Digital Image Correlation Local Algorithms

Digital Image Correlation local algorithms are based on the definition of a measurement grid and groups of pixels (subsets), which define each point of the grid. The correlation coefficient between the reference subset (i.e. the subset surrounding the measurement point on the reference image) and the deformed subset (i.e. the subset surrounding the measurement point on the deformed image) is computed. This computation is to be computed for integer pixel tentative values of the displacement to obtain a correlation map, which classifies the possible integer displacements along horizontal and vertical directions through the corresponding correlation values, in the range ±1. Finding the location of the maximum value of the correlation map provides a rough estimation of the displacement between reference and deformed images. Subsequently, subpixel accuracy in the displacement measurement can be achieved by fitting the correlation map with a specific function (generally a second-order polynomial) and then analytically or numerically determining the location of the maximum of this interpolating function. Many different implementations are available in the literature for this procedure, exploiting different interpolating functions or even nonlinear optimization to deform the subset. However, they mainly differ in the second step, i.e. the subpixel definition of the displacement, while most of them rely on a pixel-domain definition of the correlation map. To assess the effectiveness of the pixel-domain approach compared with spatial-frequency-domain computation of the correlation map, a DIC algorithm will be developed based on the simplest implementation of the subpixel displacement definition, i.e. second order polynomial form with analytical maximum detection. On the other hand, the first integer assessment step will be implemented in two different ways: by using the conventional pixel-domain approach, and by using the proposed spatial-frequency domain correlation map computation.

2.1 Pixel domain correlation map

The pixel-domain method to compute the correlation map is based on the definition of tentative integer displacements, namely u and v, which are iteratively imposed to the subset to compute the corresponding correlation factor (C_{pd}), using the equation:

$$C_{\mathrm{pd}}(u,v) = \frac{\sum_{i,j}(r(i,j)-\bar{r})(d(i-u,j-v)-\bar{d})}{\sqrt{\sum_{i,j}(r(i,j)-\bar{r})^2 \sum_{i,j}(d(i-u,j-v)-\bar{d})^2}} \quad (1)$$

where r refers to the reference image, while d refers to the deformed image. The indexes i, j denote the pixels of a subset, and the values $\bar{r}$ and $\bar{d}$ (i.e. the mean values of reference and deformed subsets) are used to normalize the correlation factor in the range of ±1. In this way, any tentative integer value of u and v would provide a value of C_{pd}, allowing to compute the correlation map. The bigger the maximum values of u and v, the larger the correlation map will be. On the other hand, larger values of displacements entail a larger searching zone, thus resulting in longer computation time. In particular, if a displacement $\bar{p}$ is expected in the data, the minimum acceptable searching zone will be ceil($|\bar{p}|$) + 1, where the ceil(·) operator refers to the upper integer of the argument, while the | · | operator refers to the absolute value.

2.2 Spatial-frequency domain correlation map

As an alternative to the conventional pixel-domain computation of the correlation map, a spatial-frequency domain method is proposed in this paper. The method relies on the circular convolution theorem [8], which demonstrates that the cross-correlation between two signals x and y can be efficiently computed by their fast Fourier transforms X and Y as follows:

$$C_{\text{fd}} = \frac{ifft(X^* \cdot Y)}{\sqrt{\max\left(ifft(X^* \cdot X)\right) \cdot \max\left(ifft(Y^* \cdot Y)\right)}} \tag{2}$$

where the symbol * denotes the complex conjugate function. If this concept is applied to the 2D subsets defined on reference and deformed images, it is possible to compute the correlation map without the need for iteratively using Eq. 1 for different values of the tentative integer displacement. Indeed, the dimensions of C_{fd} obtained with Eq. 2 are the same as the dimensions of the input subsets. This means that, if a subset of n×n pixels is considered, a n×n correlation map will be obtained, corresponding to a displacement range from -n/2 to n/2 along both horizontal and vertical directions. It is worth noting that the definition in Equation 2 relies on FFT computation also for normalization, which can be proven to be not computationally efficient. Indeed, it is possible to normalize the correlation values using the same approach as Equation 1 and to speed up the computation by normalizing C_{fd} using as a denominator the term $\sqrt{\sum_{i,j}(r(i,j)-\bar{r})^2 \sum_{i,j}\left(d(i,j)-\bar{d}\right)^2}$. In the performed trials, the latter normalization resulted to be about 30% faster with respect to the former.

2.3 Example of correlation maps

The use of the pixel-domain and the spatial-frequency domain approaches to compute the correlation maps is exemplified in Figure 1: a subset of 61 pxl was used, and a displacement of -5 pxl was imposed between two synthetic images (see Section 3.1 for details concerning the data preparation). As can be noted, the obtained correlation maps are qualitatively similar, both showing a correlation maximum in correspondence of -5 pxl in the horizontal direction. Nevertheless, the maps do not show exactly the same distributions, so that a different subpixel result is expected. In particular, the pixel domain map shows a minimum value of about -0.2, while the frequency domain map shows a minimum value of about 0.7. This can be ascribed to the fact that the pixel domain elaboration redefines the deformed subset for every tentative integer displacement, thus comparing different regions of the images. On the other hand, the frequency domain approach, based on FFTs, implicitly considers periodicity in the image, and thus only uses the data in the region of the images corresponding to the initial subsets. In either case, the first step of the displacement computation is to retrieve the indexes of the maximum of the correlation map, i.e. u_{i} and v_{i}, which correspond to the actual displacement rounded to the nearest integer. Subsequently, the subpixel accuracy can be obtained by locally interpolating the correlation map with the quadratic polynomial form.

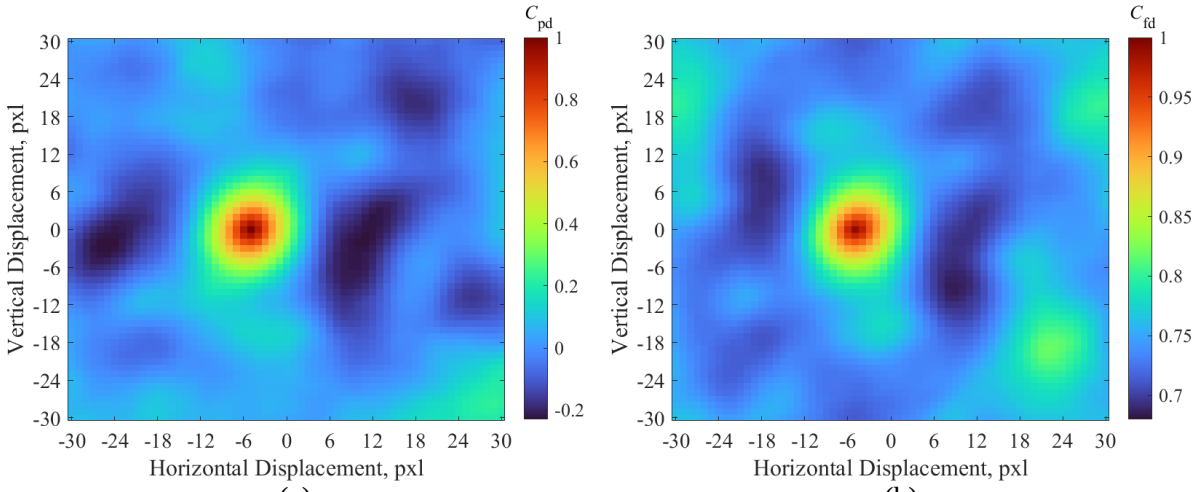

Figure 1: Examples of correlation maps for the investigated approaches: (a) pixel domain and (b) spatial-frequency domain.

3 Algorithms comparison

3.1 Synthetic dataset

A first campaign was performed on synthetic data, to have a full control on both displacement amplitudes and noise level in the image. The approach explained in [9] was followed. In particular, a synthetic speckle pattern was produced by analytically plotting a series of black ellipses with random centers and principal axis lengths on a white background. Since the plot is analytical, it was possible to precisely apply the desired displacement to all the speckles, to simulate a rigid motion. Thus, a 1×1 a-dimensional image was defined, and the a-dimensional speckles principal axis was set having a mean value of 0.05 and a standard deviation of 0.01. This vectorial image was then converted into a discretized image, simulating the acquisition by and actual camera sensor. In the provided examples, the resulting average size of the speckles is about 10 pxl, and the standard deviation is about 2 pxl. A sinusoidal displacement along the horizontal direction was imposed to the speckles, by plotting 100 frames for a full period. This procedure was repeated for increasing values of the vibration amplitude, in the range 0.01 to 10 pxl. For each simulated scenario, random noise with uniform distribution was added pixel-wise, having an amplitude of 255/10, which corresponds to 1/10 of the maximum value that an 8-bit image can store. This procedure produced a noise-free dataset and a corresponding noisy dataset, to assess the effect of noise on the algorithm performance. The production of the synthetic images is exemplified in Figure 2.

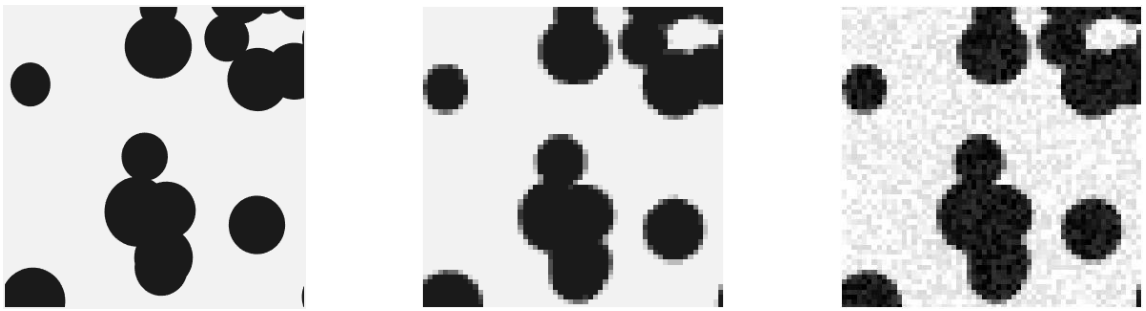

(a) (b) (c)

Figure 2 – Synthetic image generation: (a) vectorial image, (b) printed image with finite resolution and (c) printed image with added noise.

Figure 2(a) shows the vectorial image, Figure 2(b) shows the discretized frame, while Figure 2(c) shows the corresponding image with added noise. For each image set, the displacement over time was computed for a measurement point placed at the center of the image. The results obtained with the two different approaches could then be compared in terms of computational time, amplitude accuracy (i.e. difference between measured amplitude and ground truth) and signal-to-noise ratio. In particular, this latter parameter was computed using the formula:

$$\mathrm{SNR} = 10\log_{10}(\mathrm{mean}(s^2)/\mathrm{mean}(n^2)) \tag{3}$$

To apply Equation 3, it is possible to define the signal *s* by computing the FFT of the measured displacement and extracting the first harmonic component (since precisely one period is contained in the dataset), and then it is possible to retrieve the noise *n* by subtracting *s* from the measurement result.

Firstly, the computational time is considered. During the tests, all the datasets, each presenting 100 images were separately elaborated imposing one measurement point and a subset size of 61 pxl. Thus, the total time needed to elaborate each dataset was measured, and the average between the noise-free dataset and the noisy dataset was computed for each algorithm. This provided the average computational time relative to each algorithm and for each displacement amplitude. It is worth noting that the pixel-domain algorithm needs to adjust the searching zone to the expected displacement, while the frequency-domain algorithm always provides displacement maps up to the dimension of the subset (thus, ±30 pxl in this example). The results are shown in Figure 3(a), where the horizontal axis shows the imposed displacement amplitude, while the vertical axis shows the computational time. The red circles refer to the pixel-domain results, while the blue circles refer to the frequency-domain computational time. As can be noted, the pixel-domain algorithm computational time increases with the displacement amplitude, while the frequency-domain algorithm always takes the same computation time to perform the task. This is explained by the fact that the searching zone is to be increased for the pixel-domain algorithm following the expected displacement. Additionally, since the search zone increases both along vertical and horizontal directions (as in principle the actual displacement is an unknown 2D vector), this has a quadratic effect on the computational time. Indeed, the least-square-fitting quadratic polynomial was added with a red line in Figure 3(a), showing an almost perfect overlap between the computed points and the interpolation line. Finally, the blue curve was added to the plot, corresponding to the mean value of the frequency-domain computational time, demonstrating a negligible oscillation of the computed points with respect to their mean value. This proved that, for displacement amplitudes greater than about 1.5 pxl, the frequency-domain approach is faster than the pixel-domain algorithm.

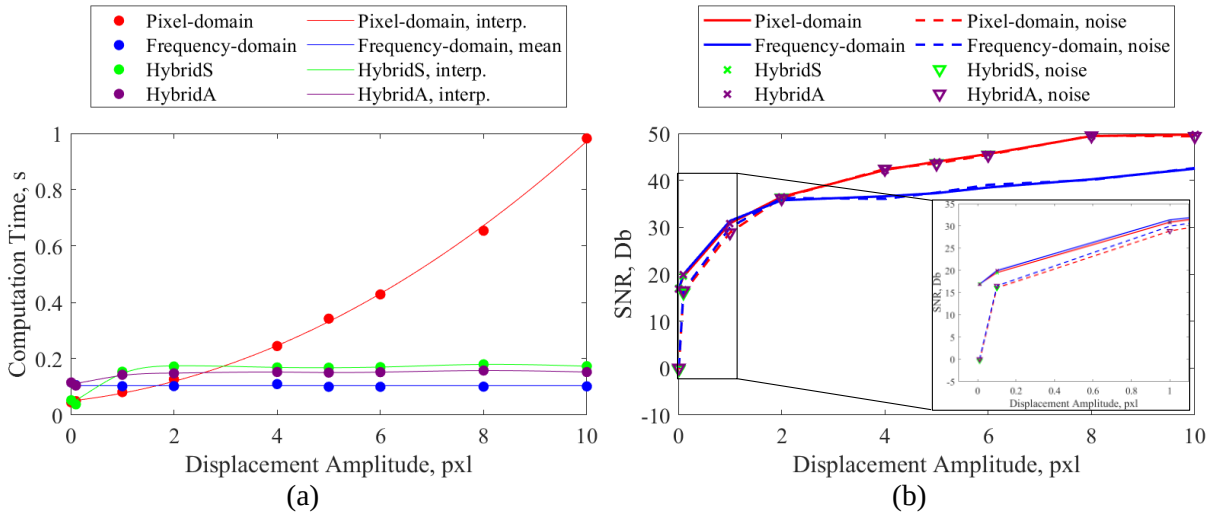

Figure 3 – Comparison between pixel-domain and frequency-domain approaches: (a) computational time and (b) SNR.

Subsequently, the signal-to-noise ratio was computed using Equation 3 for the four studied datasets. The results are reported in Figure 3(b): the solid and dashed red lines refer to the pixel-domain approach, applied to noise-free and noisy images respectively, while the solid and dashed blue lines refer to the frequency-domain approach, applied to noise-free and noisy images respectively. The plot shows that for displacements

larger than 2 pxl, the pixel-domain approach provides much better results in terms of SNR values. Nevertheless, the zoomed view of the small displacement region was added to Figure 3(b) to highlight that, for displacements lower than 2 pxl, the frequency domain algorithm performs slightly better than the pixel domain one. This means that the two approaches have complementary performances: for small displacements, the pixel-domain approach is faster but less precise, while for large displacements the frequency-domain approach is much faster but less reliable. This suggests that a hybrid approach can benefit from both advantages by selecting the proper computation method depending on the displacement amplitude. Indeed, a hybrid algorithm could be developed following the block diagram in Figure 4. Figure 4(a) refers to a hybrid algorithm that focuses on the computational time (hybrid-speed, HybridS), while Figure 4(b) refers to a hybrid algorithm that focuses on the accuracy (hybrid-accuracy, HybridA). In the following, PD will be used to denote results obtained with the pixel-domain algorithm while FD will be used for the frequency-domain results). In the case of HybridS, as a first step, the integer displacement u_i, v_i is computed by using the pixel-domain approach with a 1-pixel searching zone. Indeed, it is the fastest algorithm when a searching zone of 1 pixel is selected. Then, if the maximum lies in the middle of the correlation map, it means that the actual displacement is lower than 1 pxl, thus the subpixel routine (i.e. polynomial interpolation) can be performed to retrieve the actual displacement. On the other hand, if the maximum of the correlation map of the first step lies on the boundary of the searching zone, it means that the global maximum is farther than 1 pxl. Thus, the frequency domain algorithm (which is the fastest for large displacements) can be performed to retrieve the integer displacement value disp0 = (u_i, v_i), which then serves as a first guest for the final pixel-domain computation. This last step is performed by centering the subpixel on disp0 and defining a 1 pxl searching zone. This will provide a correlation map that can be interpolated with the polynomial form to retrieve the actual subpixel displacement. Following this procedure, the hybrid algorithm is able to determine the rounded displacement with the fastest approach, and then the final displacement is always computed by interpolating the pixel-domain correlation map, which provides the highest SNR values in the large displacement range. On the other hand, the HybridA accuracy can select the algorithm that provides the highest SNR depending on the displacement range: the integer displacement disp0 is computed using the frequency-domain approach. Subsequently, if the integer displacement is equal to 0 (i.e. actual displacement is in the subpixel range), the subpixel routine is applied to the frequency-domain correlation maps, which show the highest SNR ratios (zoomed view in Figure 3(b)). Alternatively, if disp0 is different from 0, the pixel-domain approach is used with the definition of a 1 pxl searching zone around disp0. The resulting correlation map is used to perform the subpixel routine. In other words, HybridS is equivalent to the pixel-domain approach in terms of SNR results but perform faster, while HybridA selects the approach with the highest SNR and still has improved computational times.

These procedures were implemented and tested on the synthetic dataset, obtaining the green and purple data in Figure 3. In Figure 3(a), the HybridS algorithm results are reported with green circles, while HybridA results are reported with purple circles. Additionally, the corresponding fitting splines are reported with a green and purple solid line, respectively, to highlight the trend. As can be noted, for small displacements HybridS achieves the short timing of the pixel-domain approach, while for large displacements a constant computational time was obtained. This time is considerably lower than the pixel-domain results, and only slightly higher than the frequency-domain results. This time increment is due to the fact that, for large displacement, two steps of computation with the pixel-domain algorithm are performed in addition to the frequency domain approach. Conversely, HybridA equals the timing of the frequency-domain approach in the small displacements region and shows a constant time in the large displacement regions. This constant timing is higher with respect to the frequency-domain approach, since the pixel-domain algorithm is additionally applied after determining disp0 with the frequency-domain approach, while results are much faster with respect to the pixel-domain approach, and even faster than HybridS since the pixel-domain algorithm is applied only once. On the other hand, Figure 3(b) shows the results of the hybrid approaches in terms of SNR values: the crosses refer to the noise-free dataset, and the triangles refer to the noisy data, while green and purple markers refer to HybridS and HybridA respectively. It is worth noting that the SNR values of HybridS are exactly the same as the pixel-domain algorithm, because the subpixel computation is always performed on the local correlation map obtained with the pixel-domain algorithm, while the SNR values of HybridA switches from the frequency-domain results (in the small displacements region) to the pixel-domain results (in the large displacements region).

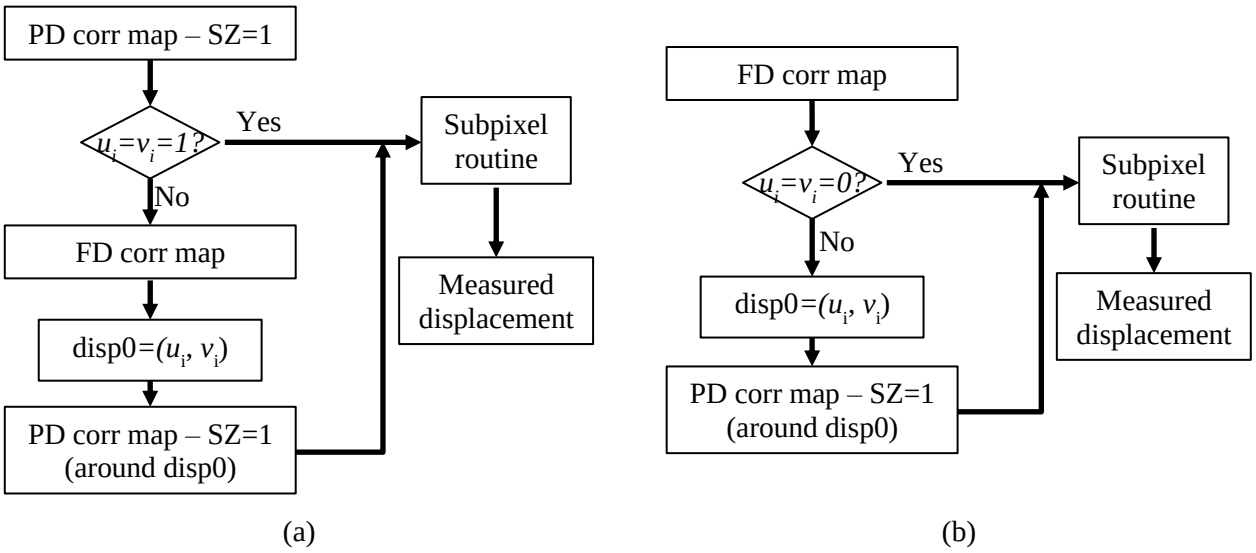

Figure 4 – Block diagram of the Hybrid DIC algorithms: (a) speed-oriented and (b) accuracy-oriented.

3.2 Experimental dataset

Even if the synthetic dataset provided an interesting insight into the two approaches, it is mandatory to also analyze actual experimental data to assess the performances on a realistic scenario. To this extent, the vibration of a cantilever plate was measured with a Digital Image Correlation setup. The setup, fully described and validated in [10], was composed of two Optomotive TREX cameras, a multimedia projector and four high power flicker-free 100 W LED modules (Stratusled). The cantilever plate (250 × 100 × 1.8 mm^3) was screwed to the shaker plate (TIRAvib TV51110). The shaker was set to excite the structure close to one of its resonance frequencies, at 591 Hz. The experimental setup is shown in Figure 5. A downsampling approach was used to perform the acquisition, as described in [10]. The test parameters were set in order to measure one full period of the vibration along the image set with 50 frames. It was then possible to apply the described algorithms on the image sets, to compare the outcomes in terms of SNR values.

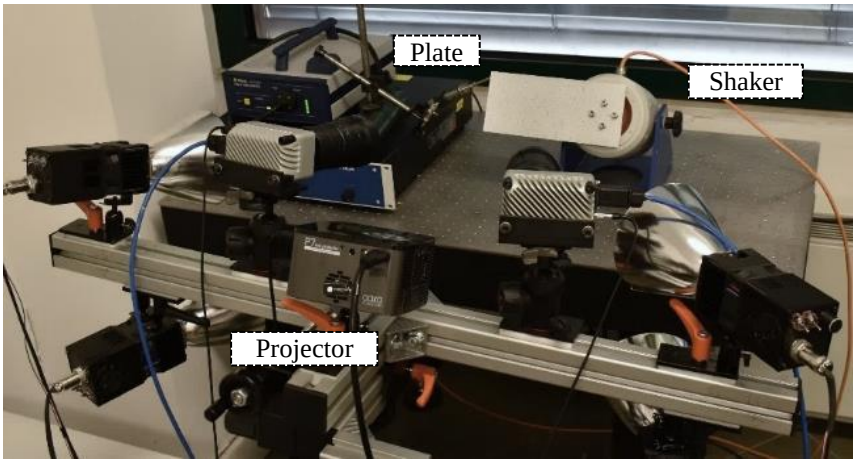

Figure 5 – Experimental DIC setup.

The elaboration was performed by using 8000 measurement points, a subset size of 21 pxl, and a search region of 4 pxl for the pixel-domain algorithm (since the maximum expected displacement was in the range of 2 pxl). The overall processing time (8000 points times 50 frames) was found to be 67.8 s for the pixel-domain algorithm, and 44.3 s for the frequency-domain algorithm, confirming that in the displacement range of 2 pxl the frequency domain approach performs faster. As an example, the displacement map along the horizontal direction, corresponding to the frame with the maximum displacement over time, is shown in Figure 6(a) for the pixel-domain algorithm and in Figure 6(b) for the frequency-domain algorithm.

Similarly to the approach in [9], the comparison was performed from two different perspectives. Firstly, each measurement point was treated as a punctual sensor in the time domain and the SNR was computed using Equation 3. This allowed plotting an SNR map, which shows the value of time-domain SNR (T-SNR) for each measurement point and for the two algorithms (i.e. pixel-domain and frequency-domain). Figure 6(c) and (d) show the results for the pixel-domain and frequency-domain algorithms, respectively. As can be seen, no relevant differences can be noted between the two plots, whose maximum and minimum values (reported on the plot for clarity) are almost the same. It is interesting to note that high SNR values are found in the region where relatively large displacements are measured, while low negative SNR values are found on the nodal line of the studied mode shape. Subsequently, the comparison was performed in the spatial domain. If a single image is considered, adjacent measurement points should have similar displacement results. Thus, a smoother map in the spatial domain corresponds to a better algorithm performance. This can be assessed by rearranging the displacement in a 1-D array and scoping measurement points from left to right and from top to bottom. An example of this procedure, for the same frame used to draw Figure 6(a) and (b), is reported in Figure 7(a) with a red line for the pixel-domain algorithm and a blue line for the frequency-domain algorithm. As can be seen, the result is composed of low spatial-frequency contributions, which represent the actual smooth deformed shape, and some high-spatial frequency components which correspond to noise. It is worth noting that a qualitative comparison highlights that the red curve has more severe spikes, corresponding to more noise. Nevertheless, the figure also shows that in the small displacement points (e.g. in the range 0 – 4500) the frequency domain is less noisy than the pixel-domain algorithm. On the other hand, in the large displacement points (e.g. in the range 4500 – 6500) the pixel domain algorithms perform better. This is coherent with the finding of Figure 3(b), which shows a better performance of the frequency-domain algorithm in the case of lower displacements, and vice versa.

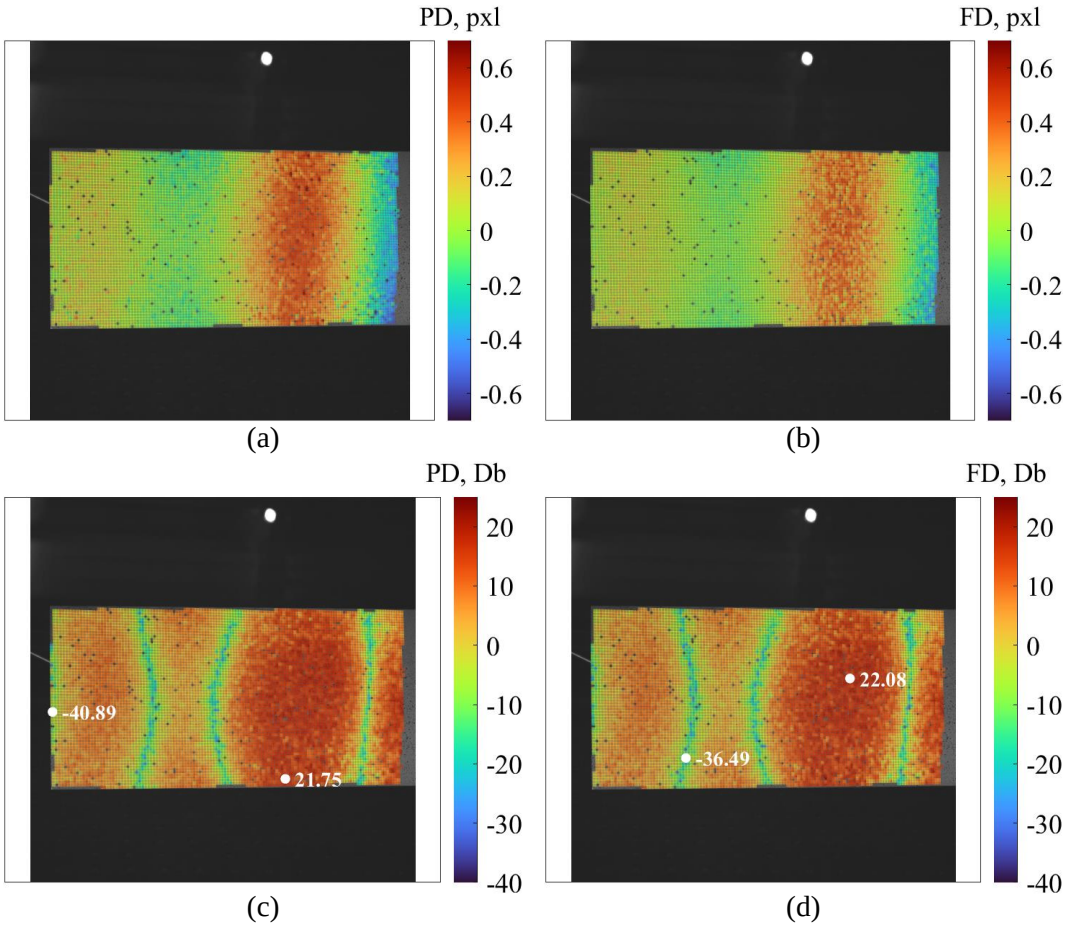

Figure 6 – Experimental DIC results: maximum displacement along the horizontal direction with (a) PD and (b) FD algorithm, (c) T-SNR using pixel-domain approach and (d) T-SNR using frequency domain approach.

This information can be condensed in a single scalar by computing the spatial SNR (S-SNR) of the data reported in Figure 7(a). Repeating this procedure for all the acquired frames, it is possible to get a picture of the overall performance of the two algorithms. The results are reported in Figure 7(b), where the red line refers to the pixel-domain algorithm while the blue line refers to the frequency-domain one. The plot confirms that the frequency-domain algorithm performs better than the pixel-domain algorithm in the small amplitude region, while the two algorithms' performance is almost the same in the large amplitude region. The computation was then repeated for the hybrid algorithms. It was found that, as expected, HybridS produced the fastest computational time (i.e. 33 s) while HybridA matched the frequency-domain timing (i.e. 42 s). Since the analyzed data were in the small displacements range, the SNR performance of HybridS and HybridA algorithms were equivalent to pixel-domain and frequency-domain values, respectively. This is shown in Figure 7(b), where the green circles refer to HybridS, while the purple circles refer to HybridA.

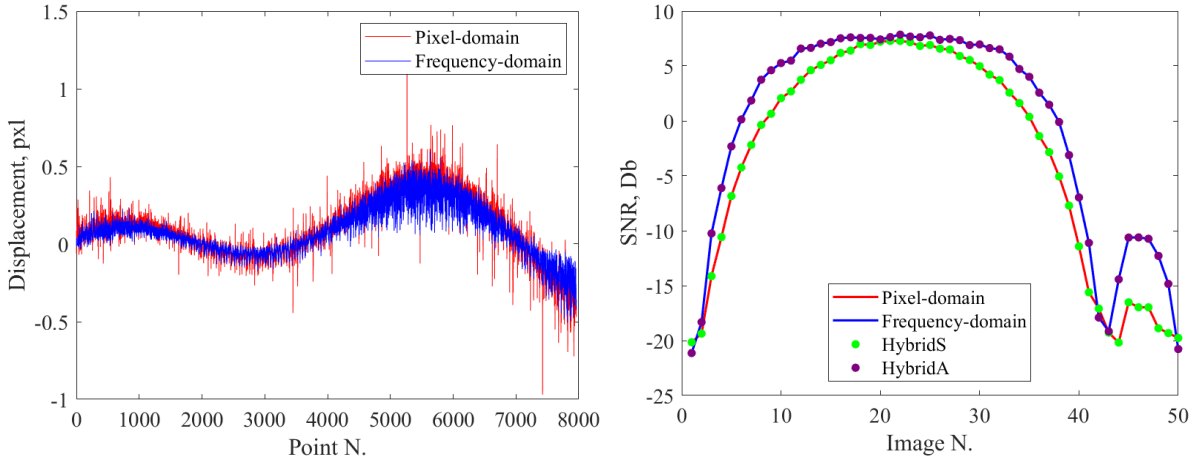

Figure 7 – Spatial domain performances: (a) displacements across the measurement points and (b) S_SNR along the time series

4 Conclusions

In this paper, two different approaches to compute the correlation map needed for Digital Image Correlation measurements are presented and discussed. The first is the conventional pixel-domain approach, which is based on the computation of the correlation map by iteratively moving the deformed subset with respect to the reference subset by integer values. The second is the frequency-domain approach, which exploits circular convolution and FFT to compute the whole correlation map with a single iteration. The investigation was initially conducted on synthetic images, obtained by analytically plotting ellipses with random dimensions and locations, and by discretizing the images to a finite resolution to reproduce the camera acquisition. The analysis showed a complementary behavior of the two algorithms in different displacement regions: for small displacements, the frequency-domain approach has a slightly higher accuracy but a slower computational time, while for large displacements the pixel-domain is much slower but has higher SNR values. Following these findings, an innovative hybrid method was proposed, with two different implementations. The first (HybridS) focuses on the computational speed, selecting the fastest algorithm depending on the displacement amplitude, while always applying the subpixel routine to local correlation maps computed with the pixel-domain approach. On the other hand, the second (HybridA) focuses on accuracy, and thus computes the correlation map by selecting the algorithm that provides the highest SNR values. Preliminary testing on the synthetic dataset confirmed that the proposed hybrid algorithms can drastically reduce computational time, especially in the case of large displacements, while guaranteeing high SNR values. Subsequently, all the studied algorithms were tested on actual experimental vibration data. This analysis confirmed that the frequency-domain approach is more accurate when applied to small displacement values, since it shows higher SNR values. The application of the proposed hybrid algorithms

confirmed that HybridS and HybridA reflect the SNR values of the pixel-domain and frequency-domain approaches, respectively, while guaranteeing faster performances.

Future developments could be focused on the application of the proposed methods to more sophisticate subpixel routines, e.g. based on image resolution augmentation or exploiting more complex interpolation functions, such as quartic polynomials or splines.

References

[1] J. Baqersad, P. Poozesh, C. Niezrecki, and P. Avitabile, "Photogrammetry and optical methods in structural dynamics - A review," *Mechanical Systems and Signal Processing*, vol. 86, pp. 17-34, Mar 1 2017.

[2] B. Pan, "Digital image correlation for surface deformation measurement: historical developments, recent advances and future goals," *Measurement Science and Technology*, vol. 29, Aug 2018.

[3] H. R. Cui, Z. M. Zeng, J. Li, H. Zhang, F. L. Yang, and S. L. Chen, "The effect of error coefficient matrices and correlation criteria on dic computation errors," *Optics and Lasers in Engineering*, vol. 174, Mar 2024.

[4] F. Barros, P. J. Sousa, P. J. Tavares, and P. M. G. P. Moreira, "Digital image correlation through image registration in the frequency domain," *Journal of Strain Analysis for Engineering Design*, vol. 53, pp. 575-583, Nov 2018.

[5] R. Zhu, D. Jiang, Z. X. Huang, L. Xie, D. H. Zhang, and Q. G. Fei, "Full-field modal identification using reliability-guided frequency-domain-based digital image correlation method based on multi-camera system," *Measurement*, vol. 211, Apr 2023.

[6] N. Dematteis and D. Giordan, "Comparison of Digital Image Correlation Methods and the Impact of Noise in Geoscience Applications," *Remote Sensing*, vol. 13, Jan 2021.

[7] C. Kopfler, S. Yoshida, and A. Ghimire, "Application of Digital Image Correlation in Space and Frequency Domains to Deformation Analysis of Polymer Film," *Materials*, vol. 15, Mar 2022.

[8] P. Stoica and R. L. Moses, *Spectral analysis of signals*: Upper Saddle River, 2005.

[9] P. Neri, "Augmented-Resolution Digital image correlation algorithm for vibration measurements," *Measurement*, vol. 231, May 31 2024.

[10] P. Neri, "Frequency-band down-sampled stereo-DIC: Beyond the limitation of single frequency excitation," *Mechanical Systems and Signal Processing*, vol. 172, p. 108980, 2022/06/01/ 2022.